Advances in Military Technology
Vol. 20, No. 1, 2025, pp. 51-66
ISSN 1802-2308, eISSN 2533-4123
DOI 10.3849/aimt.01895

Mathematical Analysis and Route Optimization for Enhanced Emitter Geolocation Using Triangulation

U. Salanturoğlu[1*] and A. G. Pakfiliz[2]

[1] *Baskent University, Ankara, Turkey*
[2] *Turkish Aeronautical Association University, Ankara, Turkey*

The manuscript was received on 16 April 2024 and was accepted after revision for publication as an original research paper on 13 March 2025.

Abstract:

This paper explores using geolocation techniques in military applications, focusing on optimizing flight maneuvers for aerial platforms to locate ground Radio Frequency (RF) threats accurately. The importance of observing the threat from wider angles to mitigate geolocation errors is emphasized. Through the analysis, the aim is to determine the optimum heading angle that enhances the precision of the geolocation technique. Determining optimal heading angle allows for an optimized route, leading to more accurate localization of RF threats. Significant improvements in geolocation accuracy were achieved by implementing route optimization, mainly by maximizing the difference between the direction of signal arrival data collected by the platform. These strategies are crucial in reducing geolocation errors and enhancing threat detection and positioning capabilities in military operations.

Keywords:

geolocation, emitter localization, triangulation, route optimization

1 Introduction

Geolocation is a technique used to determine the geographical locations of electromagnetic signal sources. This technique finds application in various domains. In military applications, geolocation plays a crucial role in identifying the positions of enemy radio communications or radar signals, enabling the passive ranging and positioning of Radio Frequency (RF) threat emitters. It is this specific application of geolocation that we are focusing on in this research. Another application domain is civilian communication. Telecommunication companies may utilize geolocation tech-

[*] *Corresponding author: Department of Electrical and Electronics Engineering, Baskent University, Ankara, Turkey. Phone: +90 534 209 62 71, E-mail: salanturogluu@gmail.com. ORCID 0009-0001-3607-8681.*

niques to ascertain RF-emitting devices' locations or to identify interfering sources disrupting their signals.

In this paper, we aim to plan flight maneuvers for a moving aerial platform used in military applications to determine the geographic locations of ground RF threats accurately and rapidly. Our goal is to enhance the location estimation performance, considering the constraints in minimizing measurement errors and enhancing precision through hardware improvements. To achieve this, we have utilized optimization algorithms to improve geolocation performance with the existing hardware. Under constrained operational conditions, our objective is to propose an optimized flight route to the pilot in terms of time and performance to execute the geolocation function. This proposal, aimed at enhancing operational efficiency, underscores the practical relevance of our research and its potential to significantly impact military operations.

2 Literature Review

In the study conducted by R. Ren and colleagues, they focused on finding an optimal route for TDOA/IFDOA geolocation sensors. The objective was to determine the most suitable route points for locating the emitter by calculating the optimal positions of TDOA/IFDOA geolocation sensors and the distances between sensors, aiming to reduce measurement errors [1].

A route planning method for locating signal sources using unmanned aerial vehicles (UAVs) is proposed by Doğancay [2]. The aim is to create a route planning algorithm to locate signal sources accurately. In the study, two fundamental methods, namely direction finding, and signal strength measurement, are employed to identify the transmission source. While the direction-finding method relies on measuring the signal from different angles, the signal strength measurement method is based on measuring the signal's strength at various points. Combining these two methods within the route planning, algorithm generates an optimal route to achieve more accurate results [2].

The study by Shahidian and Soltanizadeh [3] aimed to determine the optimal trajectory of two unmanned aerial vehicles (UAVs) for locating multiple RF signal sources. The proposed algorithm provides a roadmap requiring minimal movement and time to identify the positions of all RF signal sources. This roadmap is designed to coordinate the movements of the two UAVs, thereby enabling the rapid and accurate determination of the locations of RF sources [3].

In the study conducted by Tzoreff and Weiss [4], in scenarios involving a single sensing platform, a path has been designed to optimally collect incoming signals to determine the location of the signal source. A mathematical model has been formulated using convex optimization methods to optimize the trajectory of a single sensor. When properly configured, this model accurately determines the signal source location by identifying the path that optimally collects the signals [4].

The study by Kim [5] aimed to optimize the flight path for localization using the Line of Bearing (LOB) technique. The focus was on developing an algorithm that minimizes the movement and time required to determine the position of RF signal sources accurately. The proposed method provides a systematic approach to planning flight paths, ensuring efficient and precise localization in military applications [5].

The study conducted by Semper and Crassidis [6]. focused on utilizing a limited number of UAVs within a decentralized, distributed system to determine the location of a signal source. The research addresses the use of UAVs in scenarios where they form a network to share data and collaborate in determining the signal source location. Optimal path planning is discussed to minimize positioning errors by ensuring effective cooperation among UAVs within the network [6].

3 Review of Triangulation-Based Geolocation

One method utilized for determining the location of an electromagnetic signal source is triangulation. The primary objective of this method is to ascertain the latitude and longitude coordinates of the signal source trigonometrically by utilizing directional data of the signal source obtained from different positions of the receiving platform.

Geolocation algorithms based on the triangulation method require various data to determine the location of signal sources. A platform designed for geolocation must be equipped with hardware capable of collecting and processing these data. Hardware specifications can be determined according to the purpose of the geolocation function. Particularly in military applications, where threat positions must be defined with minimal error, hardware with high measurement accuracy is selected for military platforms. The required parameters for the geolocation algorithm, the hardware capable of measuring these parameters, and their measurement errors are given in Tab. 1.

Tab. 1 Parameters used in triangulation

Parameter	**Hardware**	**Measurement Error**
Time	GPS	20 - 30 ns
Angle of Arrival (*AoA*)	RWR	1-2°
Heading Angle of Platform	INS/GPS	< 0.1°
Location of Platform	INS/GPS	1 - 5 m

As shown in Fig. 1, the platform moves without changing its heading angle throughout the interval t_1 and t_2. The moment t_1 corresponds to when the platform obtains its initial *AoA* data. At time t_2, the platform acquires its second *AoA* data and records it along with the time and location data. The recorded data are given in Tab. 2.

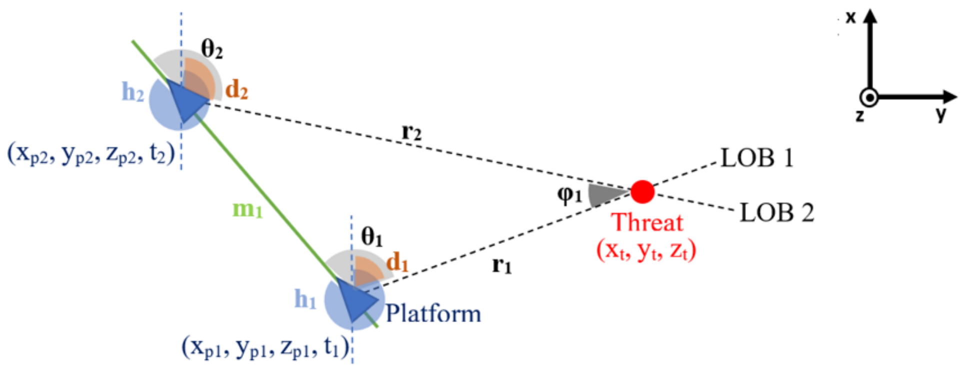

Fig. 1 Triangulation geometry

Tab. 2 Recorded data for triangulation

Time	**AoA**	**Heading Angle**	**Location**
t_1	θ_1	h_1	(x_{p1}, y_{p1}, z_{p1})
t_2	θ_2	h_2	(x_{p2}, y_{p2}, z_{p2})

The direction of the signal can be defined with respect to different references. For instance, the direction of the signal can be given regarding the Cartesian coordinate system, which takes x direction as a reference for the direction of signal arrival. This is referred to as the Direction of Arrival (*DoA*). Another representation is providing the direction of the signal for the platform's boresight. This is termed as the Angle of Arrival (*AoA*). Considering the heading angle of the platform, the transition from *DoA* to *AoA* can be calculated using Eqs (1) and (2) [7].

IF (*DoA* > *Heading Angle)*

$$AoA = DoA - Heading\ Angle \tag{1}$$

ELSE

$$AoA = 360° - Heading\ Angle - DoA \tag{2}$$

Using Eq. (3), the distance (m_1) covered by the platform can be determined based on the data provided in Tab. 2.

$$m_1 = \sqrt{\left(x_{p2} - x_{p1}\right)^2 + \left(y_{p2} - y_{p1}\right)^2} \tag{3}$$

The distance of the threat from the platform at times t_1 and t_2, denoted as r_1 and r_2, respectively, can be determined using the sine theorem provided in Eq. (4).

$$\frac{\sin\theta_1}{r_2} = \frac{\sin\left(180° - \theta_2\right)}{r_1} = \frac{\sin\varphi_1}{m_1} \tag{4}$$

$$\varphi_1 = \theta_2 - \theta_1 \tag{5}$$

$$r_1 = \frac{m_1 \sin\left(180° - \theta_2\right)}{\sin\left(\theta_2 - \theta_1\right)} \tag{6}$$

$$r_2 = \frac{m_1 \sin\theta_1}{\sin\left(\theta_2 - \theta_1\right)} \tag{7}$$

The above trigonometric equations are applicable when the platform heading angle is constant. In the scenario provided in Fig. 2, the heading angles at t_2 and t_3 differ. After applying the correction factor, the values of r_2 and r_3 can be obtained by using the sine theorem in the second triangle given in Fig. 2.

The correction factor referred to as the displacement angle, denoted as e, signifies the angular difference between the positions at t_2 and t_3 and is calculated using Eq. (8).

$$e = \arctan\frac{y_{p3} - y_{p2}}{x_{p3} - x_{p2}} \tag{8}$$

$$\theta_2' = \theta_2 + h_2 - e \tag{9}$$

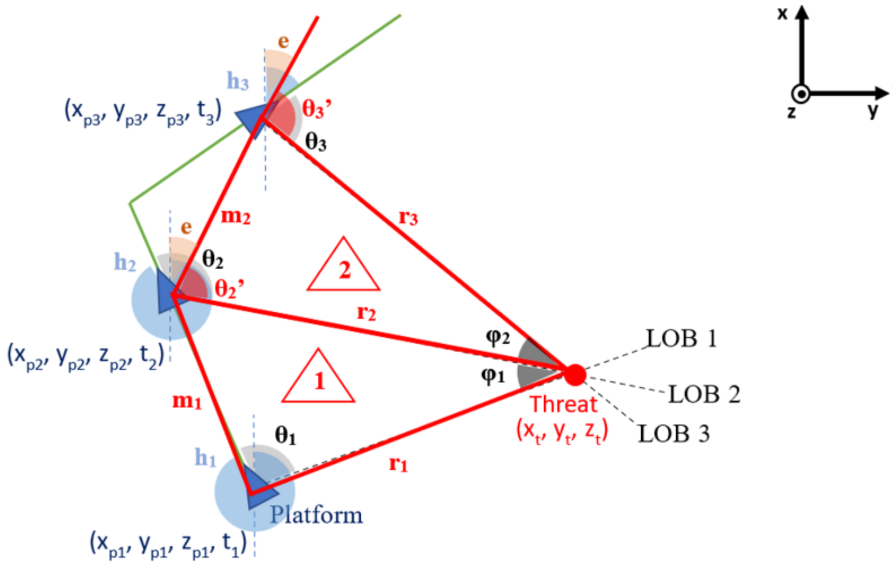

Fig. 2 Triangulation geometry for different heading angles

$$\theta_3' = \theta_3 + h_3 - e \tag{10}$$

If the heading angle does not change, the correction factor will be zero, and it will not affect the *AoA*. Therefore, the *AoA* values, denoted as θ, in the passive range calculation Eq. (6), can be replaced with the *AoA* value with the correction factor added. This algorithm can be repeated for each geolocation triangle, as in Eq. (11).

$$r_i = \frac{m_i \sin\left(180° - \theta_{i+1}'\right)}{\sin\left(\theta_{i+1}' - \theta_i'\right)} \tag{11}$$

4 Simulation Model

MATLAB was used to create the simulation environment. The simulation time interval was set to 0.1 seconds. The platform moves at a specified speed and heading angle every 0.1 seconds. The position of the signal source remains constant throughout the simulation. The platform moves within the Cartesian coordinate system. The platform's position after 0.1 seconds (Δt) can be calculated in the Cartesian plane using its speed and heading angle, as shown in Eqs (12)-(14).

$$x_{i+1} = x_i + \Delta t \cdot v_{i+1} \cdot \cos h_{\mathrm{az}_{i+1}} \cdot \cos h_{\mathrm{el}_{i+1}} \tag{12}$$

$$y_{i+1} = y_i + \Delta t \cdot v_{i+1} \cdot \sin h_{\mathrm{az}_{i+1}} \cdot \cos h_{\mathrm{el}_{i+1}} \tag{13}$$

$$z_{i+1} = z_i + \Delta t \cdot v_{i+1} \cdot \sin h_{\mathrm{el}_{i+1}} \tag{14}$$

Here, i represents the position at the first simulation point, and i+1 represents the position at the next one. The speed of the platform is denoted by v, in meters per second [m/s] units. The azimuth component of the heading angle is denoted by h_{az}, and the elevation component by h_{el}, both measured in degrees.

The direction of signal arrival relative to the signal source is calculated using Eqs (15) and (16). DoA_{az} represents the azimuth component of the direction of arrival, while DoA_{el} represents the elevation component. R, calculated using Eq. (17), denotes the slant range between the threat and the platform, while its x-y plane component is denoted as the plane range r, calculated using (18).

$$DoA_{az} = \arctan \frac{y_t - y_p}{x_t - x_p} \tag{15}$$

$$DoA_{el} = \arctan \frac{z_t - z_p}{\sqrt{\left(x_t - x_p\right)^2 + \left(y_t - y_p\right)^2}} \tag{16}$$

$$R = \sqrt{\left(x_t - x_p\right)^2 + \left(y_t - y_p\right)^2 + \left(z_t - z_p\right)^2} \tag{17}$$

$$r = \sqrt{\left(x_t - x_p\right)^2 + \left(y_t - y_p\right)^2} \tag{18}$$

The calculated direction of arrival and range values, given by Eqs (19)-(21), can be used to determine the threat's position.

$$x_t = x_p + r \cdot \cos DoA_{az} \tag{19}$$

$$y_t = y_p + r \cdot \sin DoA_{az} \tag{20}$$

$$z_t = z_p + r \cdot \tan DoA_{el} \tag{21}$$

In the absence of directional measurement errors, that is, within an environment where directional information is exact and error-free, geolocation estimates of threat positions would be highly accurate and reliable. In an ideal scenario, where there are no errors in directional measurements, and when other parameters used for threat localization, such as distance, time, and velocity, are also considered, the threat's position can be predicted with greater accuracy. Ideally, all parameters the platform measures are accurate, and all location data derived from the geolocation algorithm would converge at a single point, as illustrated in Fig. 3(a) [7].

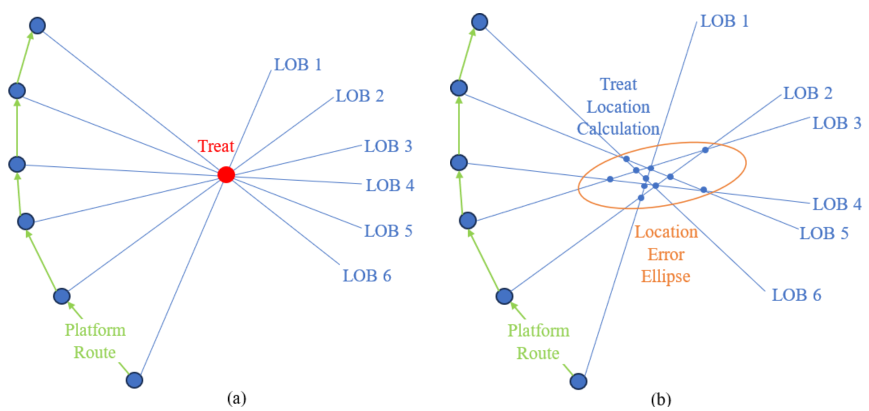

Fig. 3(a) Perfect threat location calculation (b) Treat location with error ellipse

In practice, some errors and uncertainties in directional measurements are always present. These errors can affect the determination of the threat's position and limit the accuracy of the results. In non-ideal conditions, errors in directional measurement data can arise from factors such as antenna placement, noise in the receiver, multipath effects, or errors in the platform's position and time measurements [8]. In such cases, the measured threat positions are dispersed across a particular area rather than converging at a single point, as shown in Fig. 3(b). The positions of the threats, spread across a region, can be encompassed by an ellipse with a specific confidence level, as depicted in Fig. 3(b). This ellipse is referred to as the error ellipse. The section on the calculation of error ellipses is provided in Section 5.

Gavish and Fogel [9] have investigated the effects of directional measurement errors on threat position estimation based solely on directional measurements. According to their findings, errors in directional measurement data are modeled using a Gaussian distribution with a zero mean. The standard deviation value is based on the measurement error of the directional measurement device used in the system. The 3σ directional measurement error value is approximately 2°, as provided in Tab. 1.

Directional measurement errors were added to the error-free directional measurement values, calculated using Eq. (15), resulting in inaccurate directional measurement outcomes as described by Eq. (22).

$$DoA_{\mathrm{az}} = \arctan \frac{y_{\mathrm{t}} - y_{\mathrm{p}}}{x_{\mathrm{t}} - x_{p}} + N\left(\mu, \sigma^2\right) \tag{22}$$

5 Calculation of Error Ellipse

The error ellipse is a metric that indicates how far a calculation deviates from its actual value. It is used in geographic location applications, such as geolocation, to assess the accuracy of a determined location.

To plot an error ellipse, the parameters required are the major and minor axes of the ellipse, the orientation of the ellipse, and the confidence level for the location data. The confidence level is used to calculate the sizes of the major and minor axes. Error ellipses are typically represented in a two-dimensional graph. In Fig. 4, the major ($2a$) and minor ($2b$) axes, as well as the rotation angle (ψ) of the error ellipse, define the accuracy and reliability of the calculation [10].

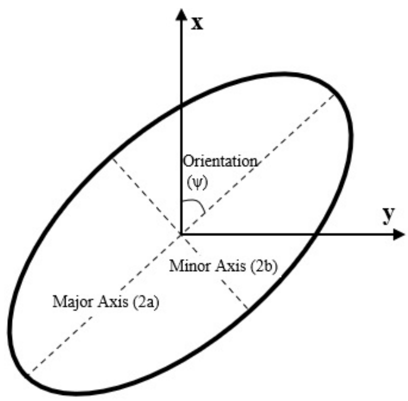

Fig. 4 Error ellipse

The equation of an ellipse with a major axis of length 2a and a minor axis of length 2b, centered at the origin, is given by Eq. (23). Here, the parameters x and y represent the position values in the coordinates x and y, respectively.

$$\left[\frac{x}{a}\right]+\left[\frac{y}{b}\right]=1 \tag{23}$$

The a and b axes are defined by the standard deviations of the data, denoted as σ_x for the x data points and σ_y for the y data points. The standard deviation measures the extent to which the data points deviate from the mean value. For a set of n data points, the standard deviation is given by Eq. (24). The mean values of the x and y data points are denoted as μ_x and μ_y, respectively.

$$\sigma_x=\sqrt{\frac{\sum_{i=1}^{n}\left(x_i-\mu_x\right)^2}{n-1}} \tag{24}$$

The value of C given in Eq. (25) is selected based on the required confidence level for plotting the ellipse. For example, for an ellipse with a 95% confidence level, which encompasses all location estimates, the value of C is 5.991. Tab. 3 presents the confidence level values for the location error ellipse.

$$\left[\frac{x}{\sigma_x}\right]+\left[\frac{y}{\sigma_y}\right]=C \tag{25}$$

Tab. 3 Confidence levels

Confidence Level	***C***
65%	2.447
90%	4.605
95%	5.991
99%	11.210

If the measurement results in x and y are not independent and there is a correlation between them, the error ellipse is oriented at an angle ψ, as shown in Fig. 4. The angle ψ is calculated using Eq. (26).

$$\tan 2\psi=\frac{2\sigma_{xy}}{\sigma_x^2+\sigma_y^2} \tag{26}$$

σ_x and σ_y represent the standard deviations of the x and y values. The term σ_{xy} refers to the covariance between these two data sets and is calculated using Eq. (27).

$$\sigma_{xy}=\frac{\sum_{i=1}^{n}\left(x_i-\mu_x\right)\left(y_i-\mu_y\right)}{n-1} \tag{27}$$

The covariance matrix determines the a and b axes of the error ellipse. It can be calculated using Eq. (28).

$$\boldsymbol{K}=\begin{pmatrix}\sigma_x^2 & \sigma_{xy}\\ \sigma_{xy} & \sigma_y^2\end{pmatrix} \tag{28}$$

The eigenvalue of the covariance matrix corresponding to the largest value, when multiplied by the confidence level C, gives the length of the major axis of the error ellipse, as shown in Eq. (29). Similarly, the eigenvalue corresponding to the smallest value, multiplied by the confidence level C, gives the length of the minor axis of the error ellipse, as shown in Eq. (30).

$$A=C\sqrt{\max\left[\text{eigenvalue}\left(\boldsymbol{K}\right)\right]} \tag{29}$$

$$B=C\sqrt{\min\left[\text{eigenvalue}\left(\boldsymbol{K}\right)\right]} \tag{30}$$

Finally, the center of the ellipse is determined which is the average of the measurement values, so it can be calculated as the average of the x and y components of the measurement values, as given by Eq. (30).

$$center=\left[\mu_x,\mu_y\right] \tag{30}$$

Circular Error Probable (*CEP*) is a concept similar to the error ellipse. In geolocation applications, the *CEP* value represents a circular area where the threat will likely be found with a specified probability. The *CEP* value can be approximately calculated using the error ellipse parameters, as given by Eq. (31). In this study, error ellipses and *CEP* values have been used to compare geolocation performance across different scenarios [10].

$$CEP\approx 0.75\sqrt{A^2+B^2} \tag{31}$$

6 Effect of Route on Geolocation

Two different flight routes have been created to examine the effect of platform movement on geolocation performance. The platform’s starting point (0, 0, 6 096) meters and the target location (50 000, 50 000, 0) meters remain the same. In the first route, the aircraft approaches the target at a 15° heading angle change every 20 seconds. The flight path for the first scenario is given in Figs 5 and 6. The simulation lasts 180 seconds, with calculations executed at the intervals of 0.1 seconds.

Fig. 7 shows the error ellipse associated with Scenario-1 and the distribution of calculated threat positions. Tab. 4 provides the required parameters for the error ellipse to encompass 95 % of the measured location data, including the major axis, minor axis, orientation, and Circular Error Probability (*CEP*) value.

Tab. 4 Error ellipse values of Scenario-1

Major Axis [m]	Minor Axis [m]	Orientation [°]	CEP [m]
69 791	3 439	57.14	52 406

In the second scenario, the aircraft moves forward by performing an S maneuver. The flight path for this scenario is given in Figs 8 and 9. The simulation lasts 180 seconds, with calculations executed at intervals of 0.1 seconds.

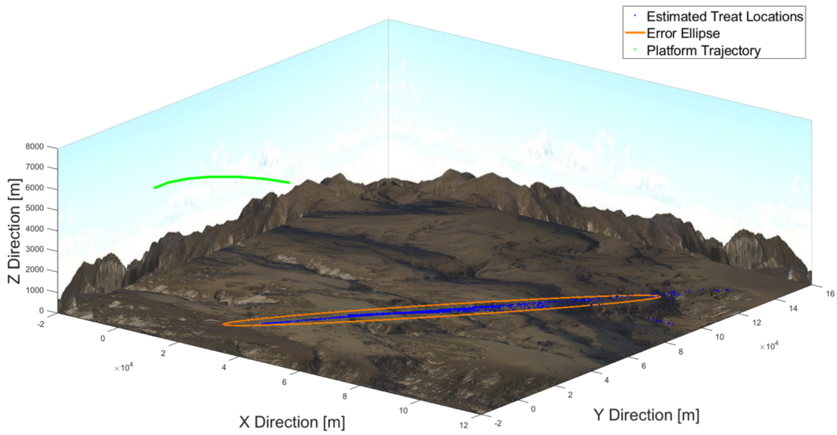

Fig. 5 Scenario-1 (xyz plane)

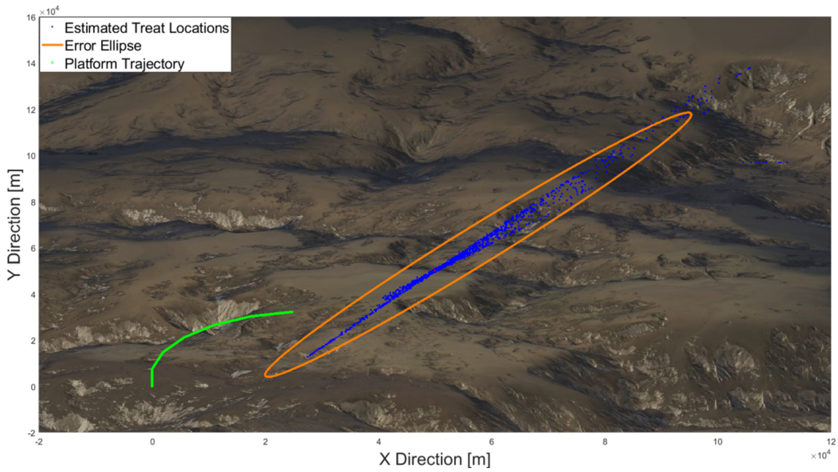

Fig. 6 Scenario-1 (xy plane)

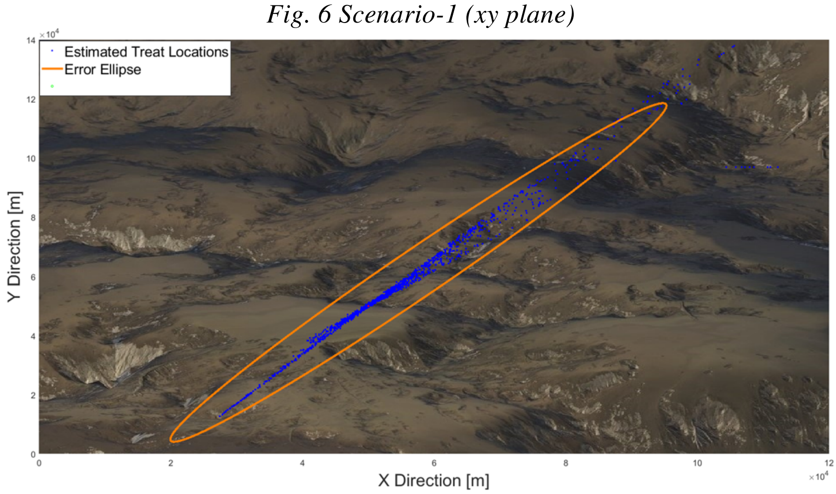

Fig. 7 Error Ellipse of Scenario-1

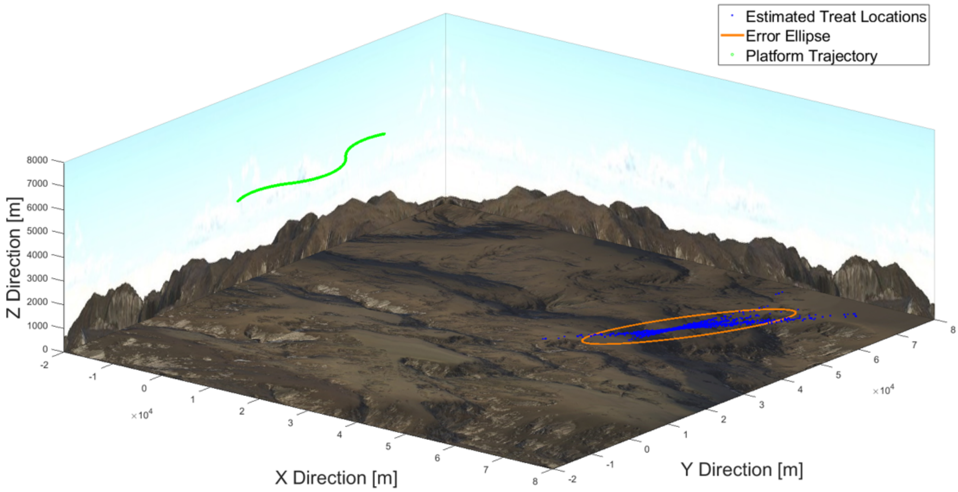

Fig. 8 Scenario-2 (xyz plane)

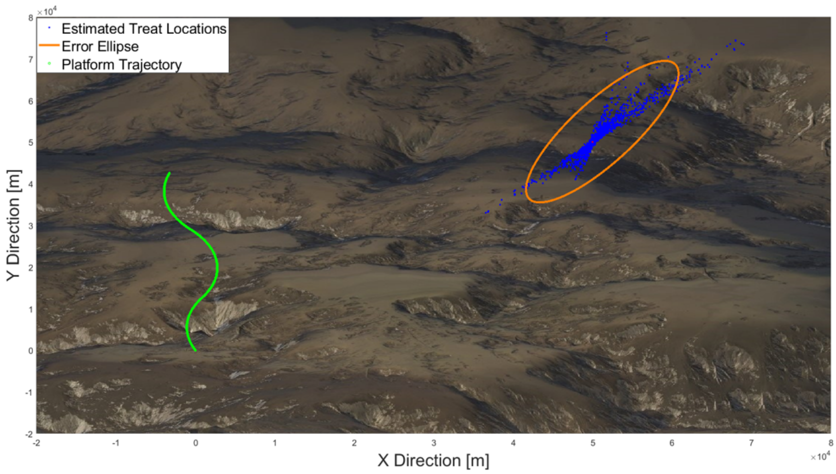

Fig. 9 Scenario-2 (xy plane)

Fig. 10 shows the error ellipse associated with Scenario-2 and the distribution of calculated threat positions. Tab. 5 provides the required parameters for the error ellipse to encompass 95 % of the measured location data, including the major axis, minor axis, orientation, and Circular Error Probable (*CEP*) value.

As seen in Tab. 4, the calculated threat positions in Scenario-1 exhibit a significant deviation. Due to the maneuver performed by the platform, the angular change in the x-axis relative to the threat is negligible. When measurement errors induced by noise are close to this angular change, a substantial deviation is observed in position calculations. Consequently, the major axis of the error ellipse indicating the error in the x-coordinate appears prominently. If the platform were to fly directly toward the threat without any angular change, it would be unable to perform the geolocation function. As seen in Scenario-2, since the platform perceives the threat from different angles and the angular difference between the measured direction data is larger, the deviation in threat position measurement is not as pronounced as in Scenario-1.

Tab. 5 Error ellipse values of Scenario-2

Major Axis [m]	Minor Axis [m]	Orientation [°]	CEP [m]
18 765	4 249	63.39	14 430

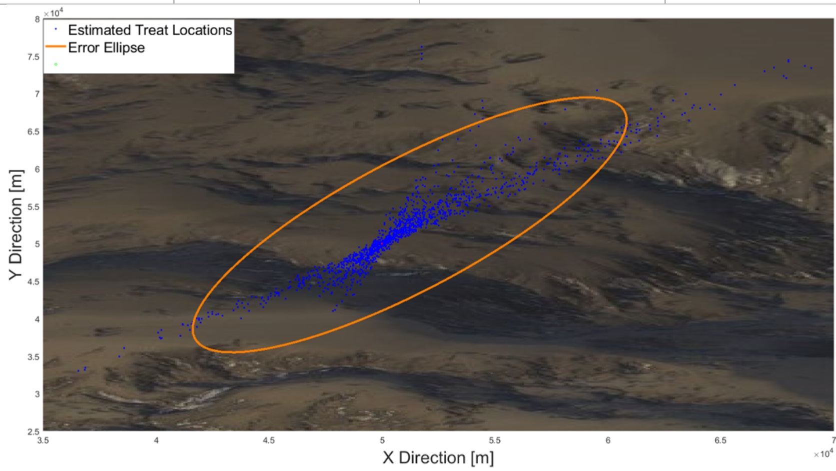

Fig. 10 Error Ellipse of Scenario-2

7 Route Optimization

Route optimization is performed to maximize the angular difference between successive threat observations, thereby enhancing the accuracy of the geolocation process. α_i is the angle created when the threat is observed from two different positions, as given in Fig. 11. To reach the maximum value of α_i, the range value R_i and the distance M_i to be travelled until the next optimization point is utilized.

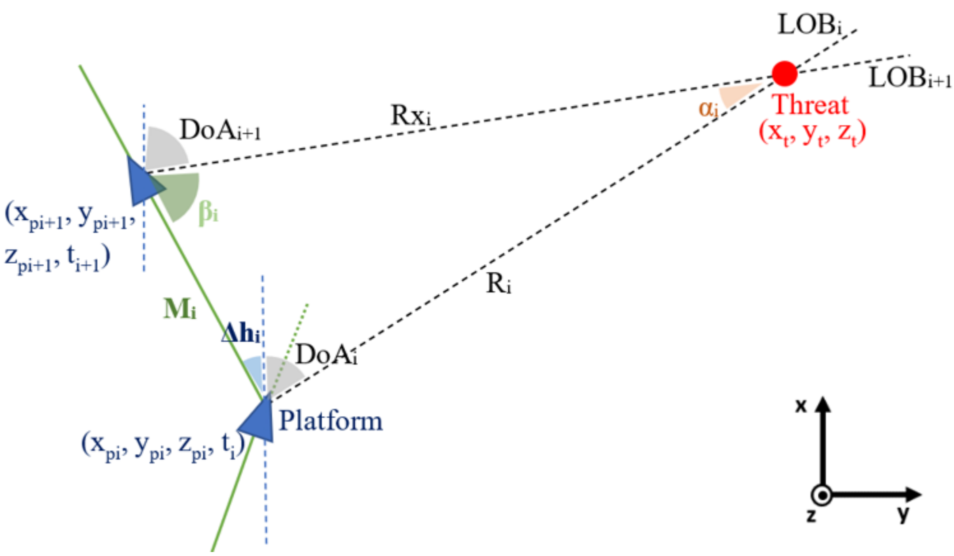

Fig. 11 Route optimization geometry for a single threat

The distance M_i that the platform needs to cover to observe the threat at angles higher than the *AoA* measurement error is associated with the distance (R_i) between the platform and the threat and the direction measurement error (DoA_{er}). The geometry required to determine the M_i value is provided in Fig. 12 and Eq. (33) can approximate the minimum value of M_i.

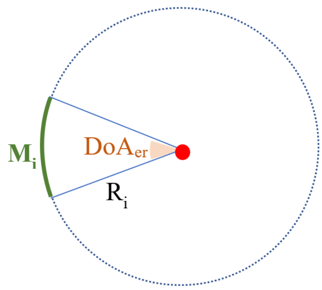

Fig. 12 Geometry to find M_i

$$M_i = 2\pi R_i \frac{DoA_{er}}{360°} \tag{32}$$

$$M_i = v_i \Delta op \tag{33}$$

As shown in Eq. (33), the product of the platform velocity (v_i) and the optimization interval (Δop) yields the displacement distance M_i until the next optimization point. It is possible to select a M_i value more than the computed one.

The α_i value can be found by applying the sine theorem to the triangle shown in Fig. 11. The Rx_i value represents the distance from the threat to the following optimization point. This value can be determined by applying the cosine theorem to the triangle provided in Fig. 11. The parameter Rx_i obtained after applying the cosine theorem is given in Eq. (35).

$$\alpha_i = \arcsin\left[\frac{M_i}{Rx_i}\sin\left(DoA_i + \Delta h_i\right)\right] \tag{34}$$

$$Rx_i = \sqrt{R_i^2 + M_i^2 - 2R_i M_i \cos\left(DoA_i + \Delta h_i\right)} \tag{35}$$

A constraint given in Eq. (37) has been added to the optimization to restrict the platform's heading angle changes. Accordingly, a maximum heading angle change of 60° can be suggested for the platform. The constraint given in Eq. (38) is included to ensure that the minimum α_i value is greater than the direction measurement error value DoA_{er}. The optimization objective function formulated for a threat is provided in Eq. (36), with the constraints given in Eqs (37) and (38).

Object Function: $$\max \alpha_i = f\left(\Delta h_i\right) = \arcsin\left[\frac{M_i}{Rx_i}\sin\left(DoA_i + \Delta h_i\right)\right] \tag{36}$$

Constraints: $$\Delta h_i = \left[-60°, 60°\right] \tag{37}$$

$$\alpha_i \geq DoA_{\mathrm{er}} \Rightarrow DoA_{\mathrm{er}} - \arcsin\left[\frac{M_i}{Rx_i}\sin\left(DoA_i + \Delta h_i\right)\right] \leq 0 \tag{38}$$

The nonlinear optimization problem provided in Eq. (36) is solved with the nonlinear constraints given in Eqs (37) and (38) to obtain the required heading angle change Δh_i for the optimal route. The new heading angle value h_{i+1} can be found in Eq. (39). Since the calculations are based on the signal's direction of arrival (*DoA*), the platform's heading angle at the time of optimization has not been considered. Similar procedures could have been conducted using the angle of arrival (*AoA*) of the signal concerning the aircraft. In such a case, the relevant calculations must consider the platform's heading angle.

$$h_{i+1} = -\Delta h_i \tag{39}$$

Before initiating route optimization, the platform maintains a straight flight for a certain duration to gather data from the threat. Using the collected data, estimated range information R_i for the threat is obtained. Once the initial range information for the threat is computed, the route optimization process begins.

In the scenario used for the nonlinear optimization solution, similar to Scenario-2, the platform's starting point is (0, 0, 6 096) meters, and the target position is (50 000, 50 000, 0) meters. Fig. 13 and Fig. 14 illustrate the route generated with the new heading angle value obtained from the nonlinear solution of the problem.

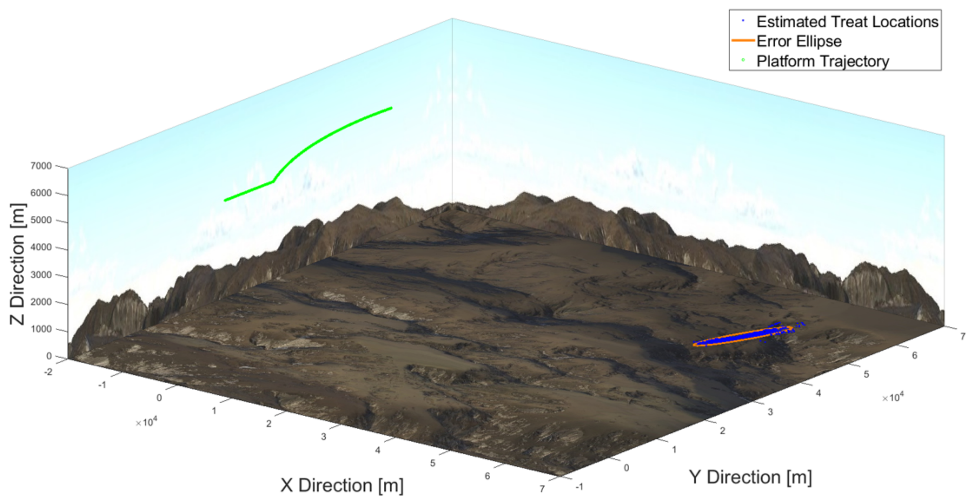

Fig. 13 Route optimization for single threat (xyz plane)

The error ellipse for the scenario with route optimization is presented in Fig. 15. The major axis length, minor axis length, orientation, and *CEP* value required to encompass 95 % of the measured position data are provided in Tab. 6.

Tab. 6 Error ellipse values of the route optimization scenario

Major Axis [m]	Minor Axis [m]	Orientation [°]	CEP [m]
7 417	1 377	66	5 657

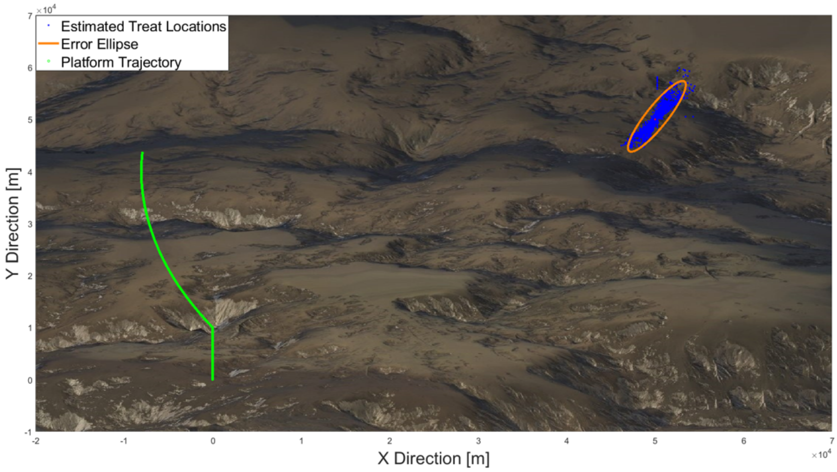

Fig. 14 Route optimization for single threat (xy plane)

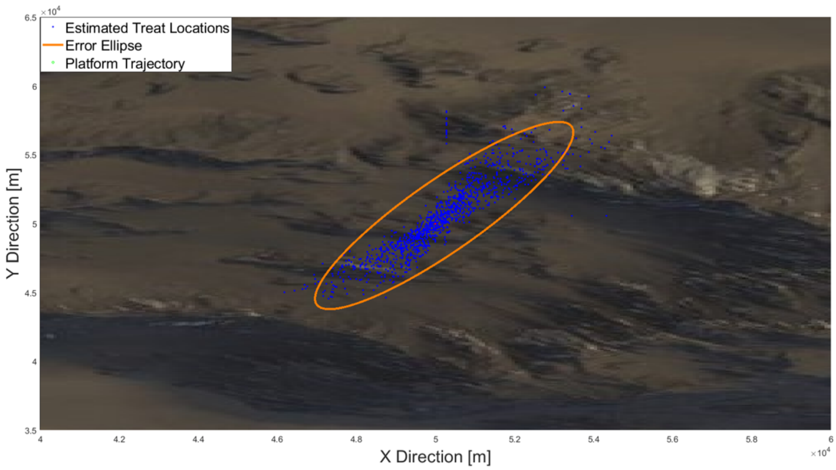

Fig. 15 Error ellipse of the route optimization scenario

When comparing the results between Scenario-2, given in Fig. 8, where the platform moves with S maneuvers, and the scenario with route optimization provided in Fig. 13, it is observed that the route optimization, aimed at maximizing the difference between the *DoA* data collected by the platform, has reduced geolocation errors.

8 Conclusion

This study explores geolocation techniques in military settings, specifically focusing on flight maneuver planning to locate ground RF threats accurately. Emphasis was placed on the necessity of broader observation angles to mitigate geographical positioning errors and to determine optimal heading angle values to enhance geolocation precision. Significant improvements in geolocation accuracy were achieved by implementing route optimization methods, mainly by maximizing the difference between

DoA data collected by the platform. When utilized to create a route, the optimal heading angle significantly enhances location determination accuracy. A comparison between a geolocation scenario with route optimization for a specific threat and a scenario without route optimization but with the same flight duration revealed a 60% reduction in the Circular Error Probable (*CEP*) value. Comparing results between scenarios with different flight routes, including maneuvers and optimized paths, notable decreases in geolocation errors were observed through route optimization strategies. These findings underscore the critical role of comprehensive observation strategies and route planning algorithms in enhancing the efficacy of geolocation techniques in military applications, ultimately contributing to improved threat detection and positioning capabilities.

References

[1] REN, R., M.L. FOWLER and E.N. WU. Finding Optimal Trajectory Points for TDOA/IFDOA Geo-Location Sensors. In: *2009 43rd Annual Conference on Information Sciences and Systems*. Baltimore: IEEE, 2009, pp. 817-822. DOI 10.1109/CISS.2009.5054830.

[2] DOĞANÇAY, K. UAV Path Planning for Passive Emitter Localization. *IEEE Transactions on Aerospace and Electronic Systems*, 2012, **48**(2), pp. 1150-1166. DOI 10.1109/TAES.2012.6178054.

[3] SHAHIDIAN, S.A.A. and H. SOLTANIZADEH. Optimal Trajectories for Two UAVs in Localization of Multiple RF Sources. *Transactions of the Institute of Measurement and Control*, 2016, **38**(8), pp. 908-916. DOI 10.1177/0142331214566026.

[4] TZOREFF, E. and A.J. WEISS. Single Sensor Path Design for Best Emitter Localization via Convex Optimization. *IEEE Transactions on Wireless Communications*, 2017, **16**(2), pp. 939-951. DOI 10.1109/TWC.2016.2635123.

[5] KIM, N. *Optimized Flight Path for Localization Using Line of Bearing* [M.S. Thesis]. Department of the Air Force, Korea Aerospace University, Goyang, 2015.

[6] SEMPER, S.R. and J.L. CRASSIDIS. Decentralized Geolocation and Optimal Path Planning Using Limited UAVs. In: *2009 12th International Conference on Information Fusion*. Seattle: IEEE, 2009, pp. 355-362. ISBN 0-9824438-0-3.

[7] ROBERTSON, S. *Practical ESM Analysis*. Norwood: Artech House, 2019. ISBN 1-63081-528-4.

[8] ELSAESSER, D. Emitter Geolocation Using Low-Accuracy Direction-Finding Sensors. In: *2009 IEEE Symposium on Computational Intelligence for Security and Defense Applications*. Ottawa: IEEE, 2009, pp. 1-7. DOI 10.1109/CISDA.2009.5356549.

[9] GAVISH, M. and E. FOGEL. Effect of Bias on Bearing-Only Target Location. *IEEE Transactions on Aerospace and Electronic Systems*, 1990, **26**(1), pp. 22-26. DOI 10.1109/7.53410.

[10] POISEL, R.A. *Electronic Warfare Target Location Methods*. 2nd ed. Norwood: Artech House, 2012. ISBN 1-60807-523-0.